

Tails of the Unexpected: The Interaction of an Isothermal Shell with a Cloud

J. M. Pittard^{1*}

¹*School of Physics and Astronomy, The University of Leeds, Woodhouse Lane, Leeds LS2 9JT, UK*

Accepted ... Received ...; in original form ...

ABSTRACT

A new mechanism for the formation of cometary tails behind dense clouds or globules is discussed. Numerical hydrodynamical models show that when a dense shell of swept-up matter overruns a cloud, material in the shell is focussed behind the cloud to form a tail. This mode of tail formation is completely distinct from other methods, which involve either the removal of material from the cloud, or shadowing from a strong, nearby source of ionization. This mechanism is relevant to the cometary tails seen in planetary nebulae and to the interaction of superbubble shells with dense clouds.

Key words: hydrodynamics – ISM:bubbles – planetary nebulae: general – planetary nebulae: individual: NGC 7293

1 INTRODUCTION

An extensive literature of analytical and numerical investigations of shock-cloud interactions now exists in which the effects of magnetic fields, radiative cooling, thermal conduction and turbulence have all been considered (see, e.g., Pittard et al. 2009; Pittard, Hartquist & Falle 2010, and references therein). However, in many astrophysical objects the cloud size is comparable to or larger than the depth of the post-shock layer, so it is surprising that to date almost all numerical investigations have been performed in the small-cloud limit where the post-shock flow has effectively an infinite depth. Notable exceptions include investigations where the global flow is simulated, for instance, in the interaction of a supernova remnant (SNR) with a cloud (Tenorio-Tagle & Różyczka 1986; Różyczka & Tenorio-Tagle 1987; Leão et al. 2009), though such models suffer from low numerical resolution. Higher resolution was used in work on the triggered collapse of a cloud by a thin shell (Boss et al. 2010), but the downstream flow was not examined. In this paper we re-examine the interaction of a cold, dense, isothermal shell with a spherical cloud, studying the effect of the shell thickness and Mach number.

2 SHELL-CLOUD INTERACTION

The shell is driven by a high pressure, low density, hot bubble. Pressure-driven shells occur in planetary nebulae (PNe) and around individual stars or groups of massive stars, and

have diameters ranging from ~ 0.1 pc to a few kpc. Since cooling breaks the scale-free nature of adiabatic simulations one is forced to choose a particular lengthscale. In this paper the interaction of a superbubble with a molecular cloud is simulated, though the results are also relevant to the smaller-scale interactions mentioned above.

The structure of the superbubble, including the thickness of the shell and the density contrast between the shell and the hot interior, can be obtained from a global hydrodynamical simulation. However, the shell properties depend on assumptions about the structure of the ISM (e.g., whether there is a density gradient, the strength and orientation of magnetic fields, the number, size and density distributions of clouds, etc.) and the efficiency of mass transfer from the cool shell and from clouds within the hot bubble to the hot, rarefied gas. Therefore, we choose instead to specify instantaneous shell and bubble properties (Mach number, surface density, bubble temperature) in order to focus on the key physics of the interaction. The shell is assumed to be planar (i.e. its radius is much larger than the cloud).

Our investigation is based around a standard model with the following parameters. The inter-cloud ISM has an assumed density and temperature of $\rho_{\text{amb}} = 3.33 \times 10^{-25}$ g cm⁻³ and $T_{\text{amb}} = 8000$ K. The density contrast of the spherical cloud $\chi = 10^3$, and its core temperature is $T_c = 8$ K. The cloud is thus in pressure equilibrium with its surroundings. To keep matters as simple as possible in this first investigation all material is assumed to behave as an ideal gas with a ratio of specific heats, $\gamma = 5/3$, although in reality the cores are molecular. This simplification has little effect on the overall dynamics. The ISM pressure $p_{\text{amb}} = 2667$ cm⁻³ K. The cloud has a mass $M_c = 300 M_\odot$ and a radius $r_c = 2$ pc. The density within the hot bubble

* E-mail: jmp@ast.leeds.ac.uk

$\rho_{\text{bub}} = \rho_{\text{amb}}/100$ ensures that this material does not appreciably cool during the simulations. We ignore thermal conduction, magnetic fields and self-gravity. Though the latter is important for the parameters we have chosen, our focus in this paper is on the development of a tail behind the cloud, rather than star formation within it.

The net heating/cooling rate per unit volume is parameterized as $\dot{e} = n\Gamma - n^2\Lambda$, where $n = \rho/m_{\text{H}} = 1.43 n_{\text{H}}$, and Γ and Λ are heating and cooling coefficients which are assumed to depend only on temperature. In the ISM, Γ decreases with increasing density as the starlight, soft X-ray, and cosmic ray flux are attenuated by the high column densities associated with dense clouds. Because the exact form of the attenuation depends on details which remain uncertain (for instance the size and abundance of PAHs), the heating rate at $T \lesssim 10^4$ K is similarly uncertain. In this work we assume that $\Gamma = 10^{-26} \text{ erg s}^{-1}$ (independent of ρ or T). The low-temperature ($T \lesssim 10^4$ K) cooling was then adjusted to give 3 thermally stable phases at thermal pressures between $2000 - 6000 \text{ cm}^{-3} \text{ K}$, as required by observations. These stable phases, at temperatures ~ 10 K, ~ 150 K and ~ 8500 K, correspond to the molecular, atomic and warm neutral/ionized phases, respectively. The cooling curve and phase diagram are shown in Fig. 1. The heating and cooling rates at low temperatures are higher than in reality, but since low temperature material is usually at high density (to maintain pressure balance) the timescale to reach equilibrium is short, and the simulations presented are not expected to be significantly affected by these simplifications.

The pressure of the shell is high enough that the gas within it should be in the cold atomic or molecular phase. However, in all the simulations the column density of the shell is much less than that of the molecular cloud, so it is assumed that the heating is high enough to keep the shell material in the warm ionized phase. Therefore, the temperature of material in the shell is prevented from cooling below 8000 K, and the shock sweeping through the ISM behaves isothermally. In contrast, material ablated from the cloud is allowed to find its own equilibrium temperature, which may be higher or lower than T_{amb} .

We adopt the density profile noted in Pittard et al. (2009) with $p_1 = 10$ (i.e. a cloud with a reasonably sharp edge). Although the cloud is initially in pressure equilibrium with its surroundings, the adopted cooling curve means that the edge of the cloud is not in a stable thermal configuration. However, the shell hits the cloud before it has time to substantially adjust itself, and the initial transient is unimportant to the following results. In contrast, the intercloud ISM is close to thermal equilibrium and its temperature remains almost constant throughout the simulation.

A key parameter for the destruction of non-magnetic, non-conducting, non-gravitating adiabatic clouds is the cloud-crushing timescale (Klein, McKee & Colella 1994),

$$t_{\text{cc}} \equiv \frac{\chi^{1/2} r_{\text{c}}}{v_{\text{s}}} = \frac{\chi^{1/2} r_{\text{c}}}{M_{\text{a}} a}, \quad (1)$$

where v_{s} and M_{a} are the speed and adiabatic Mach number of the shock through the intercloud medium having an adiabatic sound speed a . Although our study involves radiative shocks, the above characteristic timescale remains useful and is used in our analysis. All times are measured relative to when the shell is level with the cloud centre.

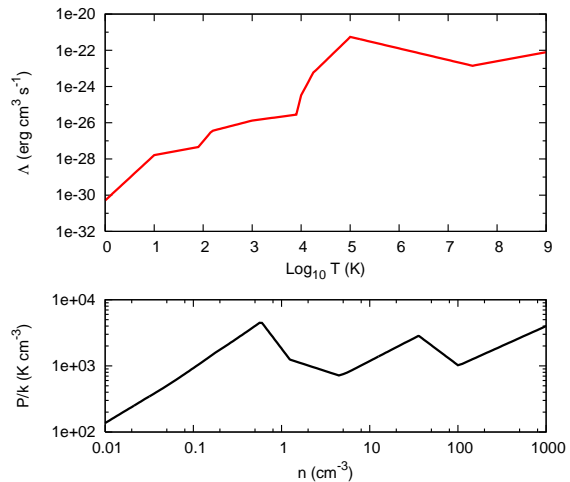


Figure 1. Top: The parameterized cooling curve adopted in this work. Bottom: The density-pressure phase diagram corresponding to the cooling curve shown and $\Gamma = 10^{-26} \text{ erg s}^{-1}$.

3 NUMERICAL SIMULATIONS

We use the MG code recently developed by Falle. It employs an exact Riemann solver for gasdynamics and piece-wise linear interpolation to achieve second order accuracy in space and time (cf. Falle 1991). Adaptive mesh refinement is handled on a cell-by-cell basis, and it is fully parallelized using MPI. Physics modules, including ones to handle self-gravity and magnetic fields, can be turned on or off as required. One such module is a $k-\epsilon$ subgrid model, which we use in this work to calculate the properties of the turbulence which is generated in high Reynolds number astrophysical flows. Such models simulate the effect that the turbulent eddies have on the mean flow by increasing the transport coefficients, particularly the viscosity, in regions where there is a lot of turbulence. Further details including the full set of equations solved can be found in Pittard et al. (2009). The 2D calculations are computed on an rz axisymmetric grid, with a domain of $0 \leq r \leq 24$, $-60 \leq z \leq 100$ for all models. 8 grid levels are used with 128 cells per cloud radius on the finest grid. A 3D calculation with a domain of $-30 \leq x \leq 30$, $0 \leq y \leq 3$, $0 \leq z \leq 3$ and 64 cells per cloud radius was also performed. The cloud is initially centered at the origin.

Fig. 2 shows the time evolution of the interaction of a 2D model with an isothermal shell of thickness $l_{\text{sh}} = 8$ pc and Mach number $M_{\text{a}} = 1.5$. The pressure and density jump in the shell is $\gamma M_{\text{a}}^2 = M_{\text{i}}^2 = 3.75$ (where M_{a} and M_{i} are respectively the adiabatic and isothermal Mach numbers of the shell). The ratio of the column density through the shell and the centre of the cloud, $\sigma_{\text{sh}}/\sigma_{\text{cl}} = 7.5 \times 10^{-3}$. Hence the cloud is relatively unaffected by the initial passage of the shell, though the shocks driven into it by the jump in the external pressure start to compress it. This compression is nearly isotropic, due to the low Mach number of the interaction and the high density contrast of the cloud. The cloud then exits through the back surface of the shell to reside in the low density interior of the hot bubble driving the shell.

The most interesting aspect of the interaction is the formation of a tail behind the cloud (for earlier simulations which display similar but much thinner tails see

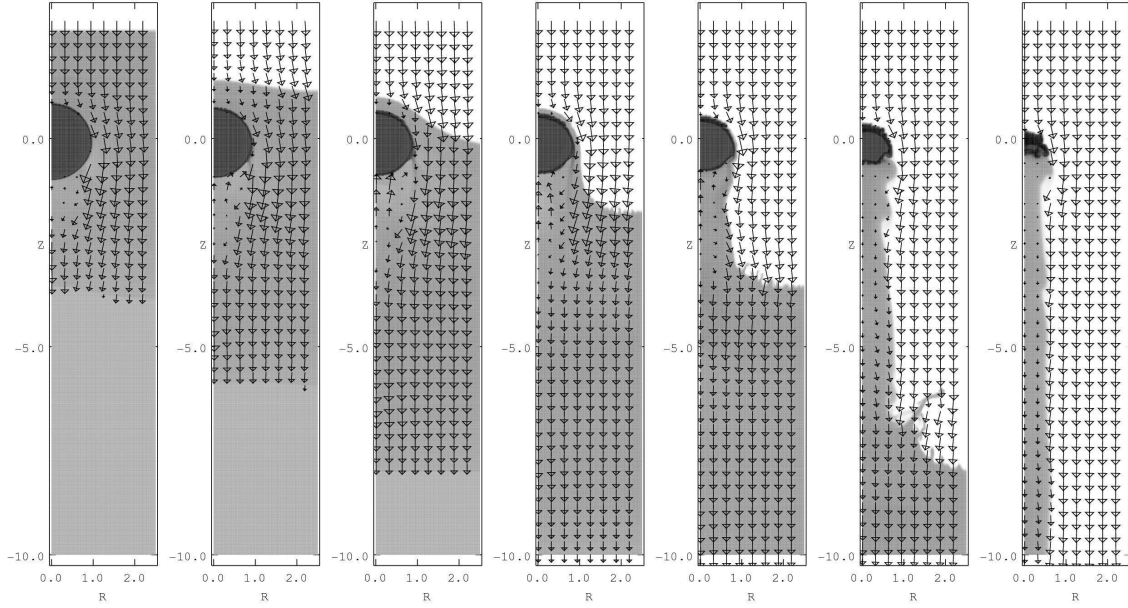


Figure 2. The time evolution of a 2D rz -axisymmetric shell-cloud interaction with $M = 1.5$, $\chi = 10^3$ and an initial shell thickness of 8 pc ($4r_c$). The interaction proceeds left to right with $t = 0.098, 0.162, 0.227, 0.291, 0.355, 0.549$ and $0.806 t_{cc}$. Material in the shell is focussed into a tail as it passes over the cloud which is compressed due to the jump in pressure. The density maps span over 5 dex: the bubble interior has $n_H = 1.5 \times 10^{-3} \text{ cm}^{-3}$ (white), the ambient medium, shell and tail have $n_H = 0.15 - 0.6 \text{ cm}^{-3}$ (light grey), and the unshocked cloud has $n_H = 150 \text{ cm}^{-3}$ (dark grey). The highest speed attained by the flow is 23.8 km s^{-1} . The unit of length is 2 pc.

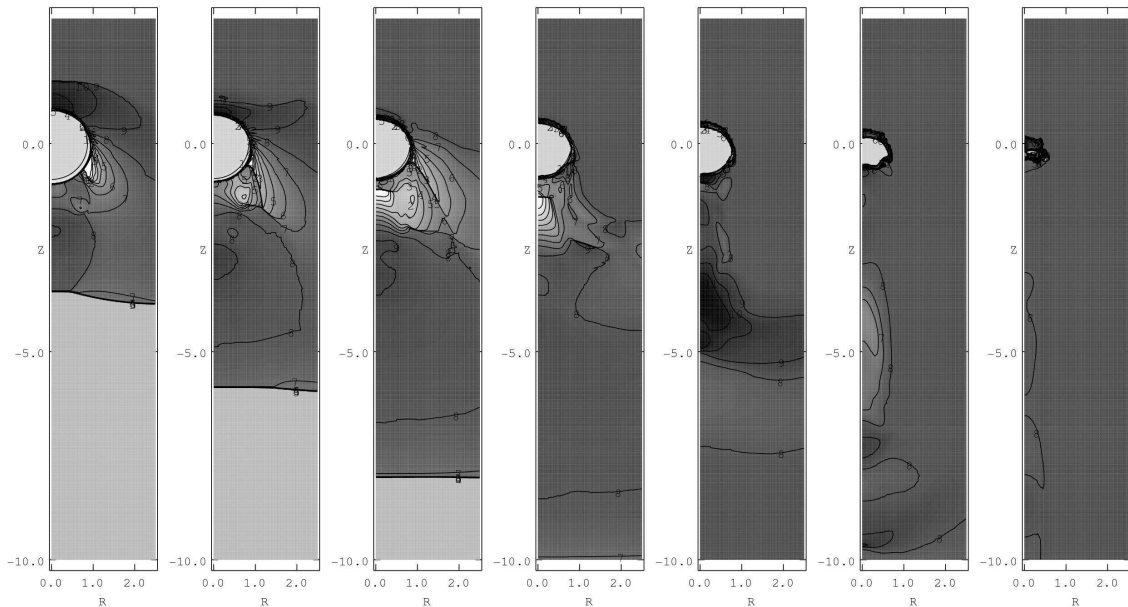


Figure 3. As Fig. 2 but showing the log of the pressure (black is high) with contour levels every 0.1 dex. The pressure gradients which exist around the cloud in the initial stages of the interaction focus material from the shell onto the symmetry axis.

Tenorio-Tagle & Różyczka 1984b). The tail is mainly composed of material from the shell, with only small amounts (less than a few percent concentration) of material ablated or stripped from the cloud. The part of the shell adjacent to the cloud moves in the lateral direction onto the axis due to the pressure gradient which exists across its face as it sweeps over the cloud (see Fig. 3). A large eddy forms which

causes this material to lose speed relative to the rest of the shell, with some material near the axis flowing back towards the rear of the cloud (see also Nittmann, Falle & Gaskell 1982; Tenorio-Tagle & Różyczka 1984a). This material is subsequently compressed against the axis by the hot, subsonic flow which overtakes it. The pressure gradient across the face of the shell diminishes as the shell moves further

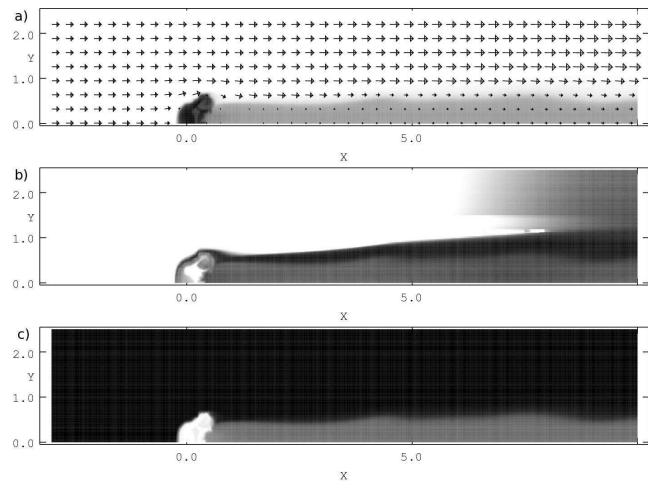


Figure 4. Same as Fig. 2, but showing cuts through the $z = 0$ plane of a 3D simulation at $t = 0.806 t_{cc}$. The shell is moving in the $+x$ direction, and there is reflection symmetry about the $y = 0$ plane. The panels show logarithmic values (black is high) of: a) the mass density and xy -velocity vectors; b) the turbulent energy density per unit mass; c) the temperature.

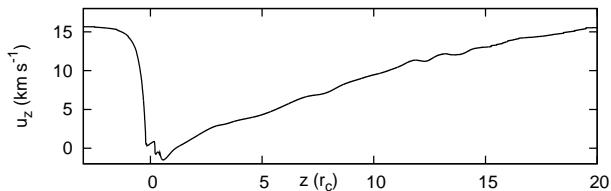


Figure 5. Velocity along the core of the tail at $t = 0.806 t_{cc}$ for the interaction shown in Fig. 2. The cloud remains near $z = 0.0$. The subsonic flow in the interior of the bubble (from the left in this plot) decelerates as it approaches the cloud.

downstream, and the focusing becomes more gradual. A 3D simulation of this interaction reveals the same features (see Fig. 4), indicating that this is a robust result which is not dependent on the assumed axisymmetry. The high shear around the cloud causes a turbulent boundary layer at the edge of the tail which grows with an opening angle of $\approx 3 - 4^\circ$. The interior parts of the tail also contain some turbulence, though the central part of the cloud has none.

The tails in these models exhibit a large length-to-width ratio which can reach nearly 50:1 at late times ($t = 2.1 t_{cc}$). Fig. 5 shows the velocity profile along the symmetry axis through the core of the tail at $t = 0.806 t_{cc}$ for the interaction shown in Fig. 2. The acceleration is approximately constant along the tail, with the velocity reaching $\approx 10 \text{ km s}^{-1}$ ($M_a = 0.8$) at $z = 10 r_c$. Due to the lack of material being stripped off the cloud, the tail eventually dissipates as it thins and then detaches from the cloud (by $t \sim 3 t_{cc}$). The axial velocity profile perpendicular to the tail shows a near constant speed at a given downstream position, which indicates efficient momentum transfer across the tail.

We have performed a series of models designed to explore parameter space to determine the conditions necessary for tail production (see Fig. 6). Decreasing the thickness of the shell (i.e. σ_{sh}/σ_{cl}) leads to a thinner tail (Fig. 6a). In-

creasing the thickness of the shell enhances the stripping of material from the cloud, which causes oscillations in the tail width (Figs. 6b and c). Interactions at higher Mach number enhance the growth of instabilities in the shear layer surrounding the tail (Fig. 6d). A model with a lower cloud density contrast ($\chi = 125$ instead of 10^3) still produces a tail (Figs. 6e-g). Tails still form behind clouds with smoother density profiles and when the shell is curved (not shown).

4 DISCUSSION

The crushing of clouds by isothermal shells has been investigated only a few times in the literature (Tenorio-Tagle & Rózyczka 1984b; Rózyczka & Tenorio-Tagle 1987; Leão et al. 2009). While these works have demonstrated that a tail composed of shell material can form in an interaction with a cloud, the shell, and consequently the focussed tail, is always much thinner than the cloud radius. Furthermore, some of the tails are short-lived while others are soon dominated by ablated material. In contrast, we emphasize that the models presented here have long-lived tails of thickness comparable to the size of the cloud.

4.1 Planetary Nebulae

Cometary tail-like structures, formed behind dense molecular clouds, are seen in many PNe. The best studied are those of the highly evolved PNe NGC 7293 (the Helix Nebula). The clouds are ionized on the parts of their surfaces exposed to the ionizing flux from the central star, and the tails point radially away from it. The tails often contain molecular material (Matsuura et al. 2009, e.g.). Two different models have been proposed to explain the tails. In “shadow” models the tail forms due to the shielding of the direct ionizing radiation field of the central star (e.g., López-Martin et al. 2001; O’Dell et al. 2005). In contrast, “stream-source” models assume that the tail forms from material photoablated from the cloud (Dyson, Hartquist & Biro 1993; Falle et al. 2002; Pittard et al. 2005; Dyson et al. 2006).

The correct model is still disputed (e.g., Dyson et al. 2006; O’Dell, Henney & Ferland 2007). However, observations of the dynamics of the tails favour stream-source models: i) there is no evidence for significant ionized gas velocities perpendicular to the tails (Meaburn et al. 1998), in contrast to the shadow model of López-Martin et al. (2001); ii) the flow accelerates along the tails (by about $8 - 14 \text{ km s}^{-1}$, see Meaburn & Boumis 2010). While our models are not specifically of the Helix tails, the velocity increase along the tail is similar to the observations, which are suggestive of a linear velocity gradient (Meaburn, private communication).

4.2 Superbubbles, Starbursts and Superwinds

The interaction of flows with clouds may be a key mechanism for producing the broad emission wings to H α line profiles seen in regions containing concentrations of massive stars including super star clusters and many giant HII regions, such as 30 Doradus (Chu & Kennicutt 1994; Melnick, Tenorio-Tagle & Terlevich 1999). Westmoquette et al. (2007a,b) concluded that the broad

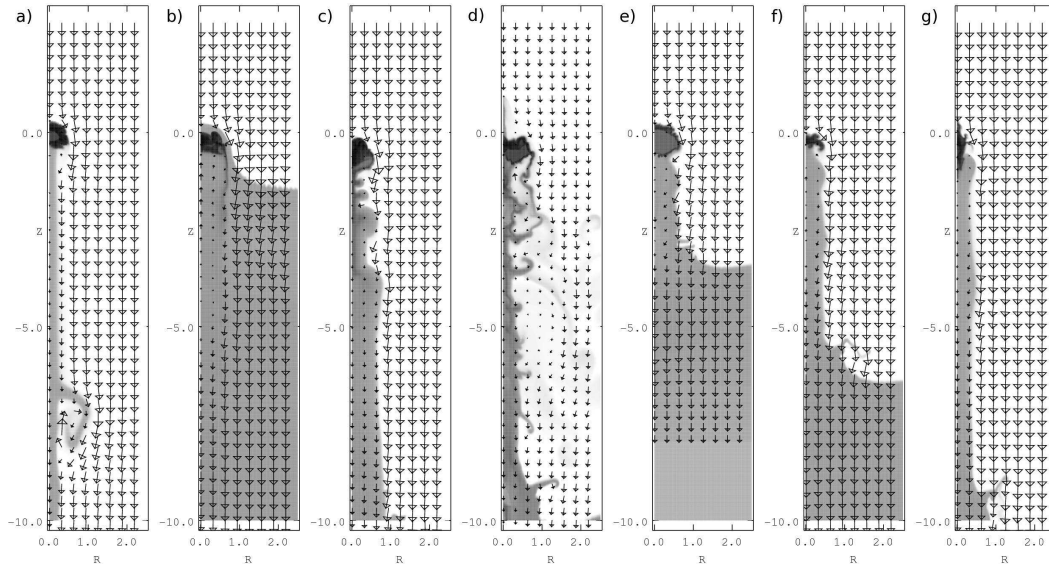


Figure 6. (a) $M = 1.5$, $l_{\text{sh}} = 2 \text{ pc } (r_c)$, $t = 0.806 t_{\text{cc}}$. (b) and (c): $M = 1.5$, $l_{\text{sh}} = 32 \text{ pc}$, $t = 0.806$ and $1.192 t_{\text{cc}}$. (d) $M = 3.0$, $l_{\text{sh}} = 8 \text{ pc}$, $t = 0.519 t_{\text{cc}}$. (e)–(g): $\chi = 125$, $M = 1.5$, $l_{\text{sh}} = 2 \text{ pc } (r_c)$, $t = 0.642$, 1.006 , and $1.552 t_{\text{cc}}$. Note that the cloud is thermally unstable in this model, and collapses to higher densities and much colder temperatures than its initial conditions. The density grey-scale is consistent in all panels, but the velocity vectors in panel d) are twice as short for a given speed compared to the other panels.

component arises in a turbulent boundary layer at the interface between hot gas flowing past cold gas stripped from clouds. However, subsequent modelling has indicated that unrealistically high flow speeds are needed (Binette et al. 2009). Instead, we believe that the broad emission wings reflect the acceleration of material along the tail and not just turbulent motions within the mixing layer.

Beautiful filamentary structures are also seen in starburst superwinds (e.g., Cecil et al. 2001; Ohya et al. 2002). While these may be material stripped from denser clouds, as seen in simulations (e.g., Cooper et al. 2008), the results in this paper indicate that some of the filaments may in fact have been formed directly out of an overrunning shell.

5 CONCLUSIONS

We have demonstrated a new mechanism for the formation of tails behind dense clouds which involves the removal and trailing of material from an overrunning isothermal shell. The mechanism appears robust to a range of shell thicknesses and Mach numbers, and the cloud density contrast, though these parameters influence the tail's properties.

REFERENCES

- Binette L., Drissen L., Úbeda L., Raga A. C., Robert C., Krongold Y., 2009, *A&A*, 500, 817
- Boss A. P., Keiser S. A., Ipatov S. I., Myhill E. A., Vanhala H. A. T., 2010, *ApJ*, 708, 1268
- Cecil G., Bland-Hawthorn J., Veilleux S., Filippenko A. V., 2001, *ApJ*, 555, 338
- Chu Y.-H., Kennicutt R. C., 1994, *ApJ*, 425, 720
- Cooper J. L., Bicknell G. V., Sutherland R. S., Bland-Hawthorn J., 2008, *ApJ*, 674, 157
- Dyson J. E., Hartquist T. W., Biro S., 1993, *MNRAS*, 261, 430
- Dyson J. E., Pittard J. M., Meaburn J., Falle S. A. E. G., 2006, *A&A*, 457, 561
- Falle S. A. E. G., 1991, *MNRAS*, 250, 581
- Falle S. A. E. G., Coker R. F., Pittard J. M., Dyson J. E., Hartquist T. W., 2002, *MNRAS*, 329, 670
- Klein R. I., McKee C. F., Colella P., 1994, *ApJ*, 420, 213
- Leão M. R. M., de Gouveia Dal Pino E. M., Falceta-Goncalves D., Melioli C., Geraissate F. G., 2009, *MNRAS*, 394, 157
- López-Martin L., Raga A. C., Mellema G., Henney W. J., Cantó J., 2001, *ApJ*, 548, 288
- Matsuura M., Speck A. K., McHunu B. M., Tanaka I., Wright N. J., Smith M. D., Zijlstra A. A., Viti S., Wesson R., 2009, *ApJ*, 700, 1067
- Meaburn J., Boumis P., 2010, *MNRAS*, 402, 381
- Meaburn J., Clayton C. A., Bryce M., Walsh J. R., Holloway A. J., Steffen W., 1998, *MNRAS*, 294, 201
- Melnick J., Tenorio-Tagle G., Terlevich R., 1999, *MNRAS*, 302, 677
- Nittmann J., Falle S. A. E. G., Gaskell P. H., 1982, *MNRAS*, 201, 833
- O'Dell C. R., Henney W. J., Ferland G. J., 2005, *AJ*, 130, 172
- O'Dell C. R., Henney W. J., Ferland G. J., 2007, *AJ*, 133, 2343
- Ohya Y., et al., 2002, *PASJ*, 54, 891
- Pittard J. M., Dyson J. E., Falle S. A. E. G., Hartquist T. W., 2005, *MNRAS*, 361, 1077
- Pittard J. M., Falle S. A. E. G., Hartquist T. W., Dyson J. E., 2009, *MNRAS*, 394, 1351
- Pittard J. M., Hartquist T. W., Falle S. A. E. G., 2010, *MNRAS*, 405, 821
- Rózycka M., Tenorio-Tagle G., 1987, *A&A*, 176, 329

- Tenorio-Tagle G., Różyczka M., 1984a, *A&A*, 137, 276
Tenorio-Tagle G., Różyczka M., 1984b, *A&A*, 141, 351
Tenorio-Tagle G., Różyczka M., 1986, *A&A*, 155, 120
Westmoquette M. S., Exter K. M., Smith L. J., Gallagher
J. S., III, 2007a, *MNRAS*, 381, 894
Westmoquette M. S., Smith L. J., Gallagher J. S., III,
O'Connell R. W., Rosario D. J., de Grijs R., 2007b, *ApJ*,
671, 358